Journal of Solid State Chemistry 183 (2010) 1785–1789

Contents lists available at ScienceDirect

Journal of Solid State Chemistry

journal homepage: www.elsevier.com/locate/jssc

Synthesis of Li_2PtH_6 using high pressure: Completion of the homologous series A_2PtH_6 (A=alkali metal)

Kati Puhakainen, Emil Stoyanov, Michael J. Evans, Kurt Leinenweber, Ulrich Häussermann *

Department of Chemistry and Biochemistry, Arizona State University, Tempe, AZ 85287-1604, USA

ARTICLE INFO

Article history:
Received 28 March 2010
Received in revised form
24 May 2010
Accepted 30 May 2010
Available online 8 June 2010

Keywords:
High pressure materials synthesis
Multi-anvil techniques
Complex transition metal hydrides

ABSTRACT

Li_2PtH_6, the missing member of the complex transition metal hydride series A_2PtH_6 (A=alkali metal), was prepared by reacting mixtures of LiH and Pt in the presence of BH_3NH_3 as hydrogen source at pressures above 8 GPa. According to powder X-ray diffraction analysis, Li_2PtH_6 is isostructural to its heavier homologues and crystallizes in the cubic K_2PtCl_6 structure (space group $Fm\bar{3}m$, a=6.7681(3), Z=4). However, PtH_6^{2-} octahedral complexes in Li_2PtH_6 approach each other closely and its structure may likewise be regarded as a defective perovskite structure where half of the octahedrally coordinated atoms (cations) are missing. The IR spectrum of Li_2PtH_6 reveals the Pt–H T_{1u} stretch and bend at 1840 and 889 cm^{-1}, respectively.

1. Introduction

Complex transition metal hydrides are a peculiar class of solid state compounds, which consist of homoleptic hydrido complexes $[TH_n]^{m-}$ and active metal (alkali, alkaline earth, rare earth) cations [1,2]. Typically the transition metal T is from groups 7 to 10. The complex anions $[TH_n]^{m-}$, in which hydridic H is covalently bonded to T, exhibit a perplexing range of coordination numbers and geometries [3]. An interesting feature is the occurrence of low formal oxidation states of T with a ligand (H^-) that does not afford the conventional "π-back-donation" mechanism. This is especially seen with group 10 metals (e.g. tetrahedral NiH_4^{4-}, trigonal planar PdH_3^{3-}, or linear PdH_2^{2-} with zero-valent T) where tetrahedral complexes with zero-valent Ni and Pd show extraordinarily weak T–H bonds [4]. Thus actual bonding situations can be intricate and sometimes the cation environment plays a decisive role in stabilizing such complexes [5].

Complex transition metal hydrides are conveniently prepared by hot sintering active metal hydrides with the corresponding transition metal in a hydrogen atmosphere employing autoclave techniques [6]. The hydrogen pressure applied will often determine the oxidation state of T and its coordination number in the hydrido complex. For example, Na_2PdH_2 with linear complex ions $Pd(0)H_2^{2-}$ forms at hydrogen pressures below 100 bar (10 MPa) [7], while Na_2PdH_4 with square planar $Pd(II)H_4^{2-}$ requires kbar pressures (above 180 MPa) [8]. Similarly, Na_2PtH_4 is obtained at pressures below 1 MPa [9], while pressures in excess of 150 MPa afford Na_2PtH_6 with octahedral $Pt(IV)H_6^{2-}$ complex ions [10].

While the synthesis conditions applied for Na_2PtH_6 also yield the heavier homologues A_2PtH_6 (A=K–Cs) [11,12], for A=Li $Li_5Pt_2H_9$ is obtained [13]. This compound contains the complex anion $Pt_2H_9^{5-}$ in which two square planar entities PtH_4^{2-} are bridged by H^-. Thus, for A=Li platinum remains in the oxidation state II. Recently Parker et al. [14] provided a comparative analysis of the series A_2PtH_6 while performing a detailed study of the vibrational properties of Rb_2PtH_6 and Rb_2PtD_6. These authors suggested that the missing start member, Li_2PtH_6, should be accessible when applying even higher hydrogen pressures.

High hydrogen pressures offer exciting prospects for metal hydride synthesis because the activity of hydrogen fluid increases sharply above 1 GPa [15]. The pressure limit of autoclave techniques may be around 500 MPa (0.5 GPa), especially when simultaneous high temperatures (up to 700 °C) are applied [6]. Pressures well above 10 GPa are accessible with diamond anvil cells (DACs) [16]. However, the DAC is not a practical tool for synthesis because of the small sample size and, in the particular case of hydrogenation reactions, the difficulties associated with loading elemental H_2. A more feasible high pressure strategy for metal hydride synthesis is the utilization of multi-anvil (MA) [17] or toroid devices [18], which provide larger sample volumes. Hydrogen is introduced via an internal source that releases irreversibly H_2 when heating the pressurized sample. Pressures are usually restricted to around 10 GPa. When employing an internal source, hydrogen activity does not relate directly to applied pressure as it is the case for H_2 loaded autoclaves or DACs [19]; the hydrogen concentration provided by a source is rather low.

* Corresponding author.
E-mail address: Ulrich.Haussermann@asu.edu (U. Häussermann).

0022-4596/$ - see front matter © 2010 Elsevier Inc. All rights reserved.
doi:10.1016/j.jssc.2010.05.033

Here we show that Li_2PtH_6 can be readily obtained by hydrogenating mixtures of LiH and Pt in a MA device. The structural properties of Li_2PtH_6 fit perfectly the trend of A_2PtH_6 compounds, which, however, results in a peculiar H substructure for A=Li. For synthesizing Li_2PtH_6 we facilitated MA gigapascal hydrogenations by introducing ammonia borane, BH_3NH_3, as superior internal hydrogen source, and by employing recently developed large-volume pressure cells [20].

2. Results and discussion

High pressure hydrogenations for metal hydride synthesis were pioneered by Russian researchers using toroid type devices [21] and later followed up by Japanese research groups using more common MA techniques [22]. In particular, it was shown that middle and late transition metals T – for which hydrides had not been known – form compounds $TH_{\sim 1}$ (e.g FeH, MoH, NiH) when pressures between 1 and 9 GPa are applied. These hydrides are recoverable and metastable at liquid nitrogen temperature. Further examples include the synthesis of a vacancy-ordered Pd hydride (Pd_3VacH_4) at a pressure of 5 GPa [23] and the formation of AlH_3 from the elements (at 9 GPa) [24]. Attempts to prepare ternary hydrides by high pressure hydrogenations, however, resulted only in few conclusively characterized products [25].

An important ingredient to high pressure hydrogenations is the hydrogen source being part of the sample. Ideally this source releases H_2 rapidly and irreversibly at slightly elevated temperatures (preferably below 300 °C) and the decomposition residual is inert toward the metal or intermetallic precursor to be hydrogenated as well as the resulting hydride. Hitherto employed sources such as $NaBH_4+2Ca(OH)_2 \rightarrow NaBO_2+2CaO+4H_2$, $LiAlH_4 \rightarrow LiH+Al+3/2H_2$, or $AlH_3 \rightarrow Al+3/2H_2$ all have drawbacks in this respect. Also, the decomposition behavior of a source under high pressure conditions is usually not known.

We perform high pressure hydrogenations in a MA device and employ ammonia borane (BH_3NH_3) as internal hydrogen source. BH_3NH_3 is isoelectronic to ethane but due to its intermolecular dihydrogen bonding it is a crystalline solid. The effects of high pressure (up to 9 GPa) on the thermal decomposition of BH_3NH_3 have been recently studied. In contrast with the three-step decomposition at ambient pressure, thermolysis under pressure releases irreversibly almost the entire hydrogen content of the molecule in two distinct steps [26]. The residual after the second decomposition, where two equivalents of hydrogen are released, corresponds to a derivate of hexagonal BN. The temperature of the second decomposition step increases from 180 °C at 1 GPa to about 320 °C at 9 GPa. With its high hydrogen capacity and well-defined decomposition behavior leading to inert residuals, BH_3NH_3 appears as superior internal hydrogen source for high pressure hydrogenations. Also, the isotopologue BD_3ND_3 can be easily prepared [27], which allows access to deuterized samples for e.g. neutron diffraction studies.

For MA hydrogenations the precursor material is pressed into a pellet which in turn is sandwiched between two pellets of BH_3NH_3. The three-pellet arrangement is sealed in a NaCl container. In contrast with sources yielding reactive intermediates/residuals no protective separator between source and sample is needed. NaCl is a popular capsule material because it provides tight seals in the case of air/moisture sensitive precursors and resists hydrogen diffusion. In our lab we apply two differently sized NaCl capsules. Their dimensions (inner diameter × length) are either 4×8 mm^2 (V=82 mm^3) or 6.15×8 mm^2 (V=238 mm^3) for attainable pressures slightly above 10 GPa and up to 7 GPa, respectively. This represents an excellent pressure–volume capability for MA techniques [20].

Highly crystalline Li_2PtH_6 was obtained with a purity of > 80% from reaction mixtures LiH:Pt:BH_3NH_3=3:1:3.333 at pressures above 8 GPa and temperatures between 450 and 500 °C. The powder X-ray pattern is shown in Fig. 1. The amount of hydrogen source corresponded to a theoretical molar ratio Pt:H_2=1:10. As a side product the intermetallic compound $LiPt_7$, which crystallizes in a $2 \times 2 \times 2$ superstructure of the simple fcc structure [28], was identified. Compared to Li_2PtH_6 $LiPt_7$ appears poorly crystalline which could indicate the incorporation of some hydrogen. Li_2PtH_6 forms also when using a stoichiometric ratio LiH:Pt=2:1 and/or lower pressures (down to 5 GPa). However, at these conditions the amount of side product is substantially increased. Further increasing the excess of LiH did not improve the yield of Li_2PtH_6. It appears that the formation of $LiPt_7$ competes with the formation of Li_2PtH_6 and the latter is favored by applying an excess of LiH and higher pressures. To support this hypothesis we attempted the synthesis of Na_2PtH_6 by MA hydrogenation using the same reaction temperature and Pt:BH_3NH_3 ratio as in the Li_2PtH_6 experiments. $NaPt_7$ does not exist and a reaction performed at 5 GPa with a stoichiometric ratio NaH:Pt=2:1 yielded quantitatively Na_2PtH_6.

According to its powder X-ray diffraction pattern Li_2PtH_6 is isostructural to the heavier homologues A_2PtH_6 (A=Na–Cs), which crystallize in the cubic K_2PtCl_6 structure type (space group $Fm\bar{3}m$, cf. Table 1). This structure corresponds to a CaF_2-type arrangement of PtH_6^{2-} octahedral units and alkali metal (A) cations, which are coordinated by 12 H-ions (i.e. by four tetrahedrally arranged faces from four different octahedra). Accordingly, the Pt and A-type atoms (ions) occupy the special positions 4a (0,0,0) and 8c (1/4,1/4,1/4), respectively, while the H

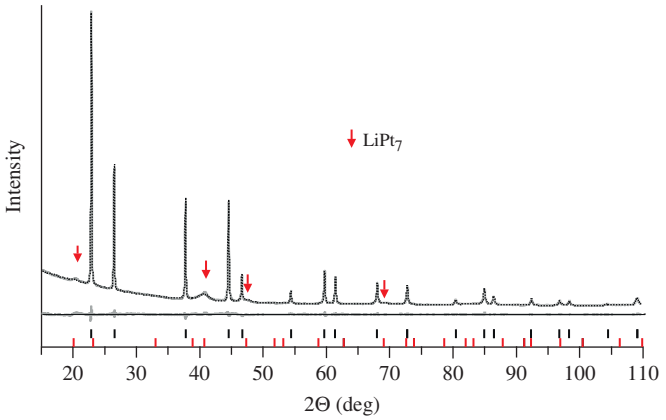

Fig. 1. The Rietveld fit to the X-ray powder diffraction pattern of Li_2PtH_6 (Cu$K\alpha_1$). The grey line represents the measured pattern, the dotted black line the calculated one. Bragg peak positions are marked by horizontal bars (black: Li_2PtH_6; red: side product $LiPt_7$). (For interpretation of the references to color in this figure legend, the reader is referred to the web version of this article.)

Table 1
Crystal data and structure refinement of Li_2PtH_6.

Compound	Li_2PtH_6
Space group	$Fm\bar{3}m$
Z	4
a, Å	6.7681(3)
V, Å^3	310.0(1)
Temp, K	295
χ^2	1.73
R_P, %	2.84
R_{wp}, %	3.78
R_B, %	1.22

position 24*e* (*x*,0,0) represents the only flexible structural parameter. Although deuterized samples (from LiD/Pt/BD_3ND_3) can be prepared using the same conditions as for Li_2PtH_6, the high pressures necessary for obtaining high yield samples (> 8 GPa) prohibited the preparation of a sample volume large enough for neutron diffraction measurements. Therefore we were not able to determine the H(D) atom positional parameter experimentally.

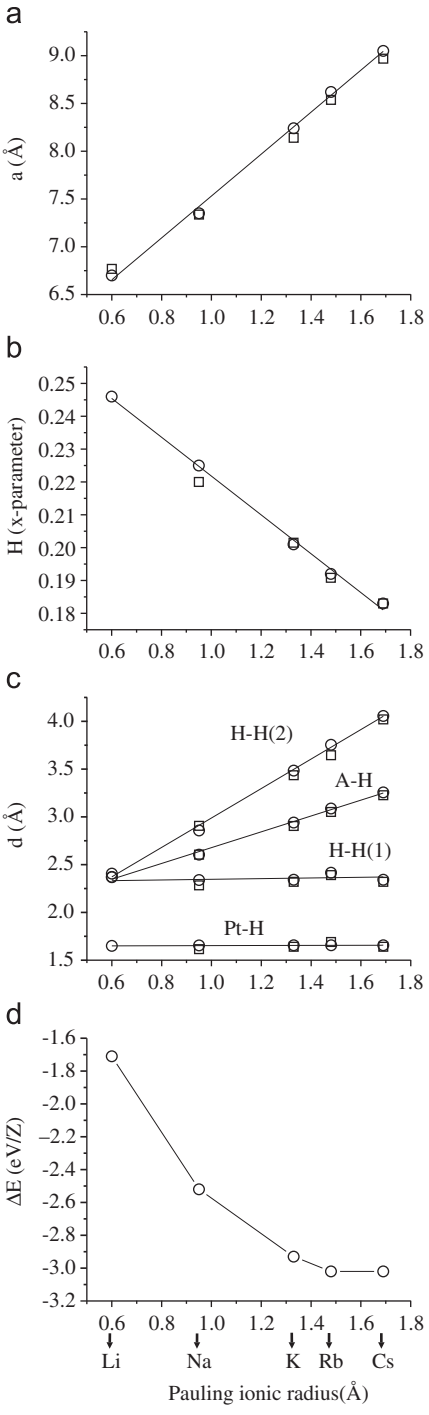

Fig. 2. Lattice parameter (a), H atom *x* parameter (b), and interatomic distances (c) for the series A_2PtH_6 (*A*=alkali metal) as a function of the Pauling ionic radius of *A*. Theoretical and experimental values (this work, Refs. [10–12]) are denoted as circles and squares, respectively. The lines are least square fits to the theoretical values (correlation coefficients > 0.995). H–H(1) and H–H(2) denote H–H distances within and between octahedral units, respectively. In (d) the computed zero-temperature formation energy for the reaction $2AH+Pt+2H_2 \rightarrow A_2PtH_6$ is shown.

Instead, we performed an optimization of the K_2PtCl_6 structure for Li_2PtH_6 by first principles calculations using density functional theory. In this study we also included the heavier homologues. Fig. 2 summarizes the result.

The structural trend in the series A_2PtH_6 (Fig. 2a–c) correlates well with the Pauling ionic radii of *A*. This has already been suggested in Ref. [14]. The agreement between experimental parameters (where available) and computed ones is very good with perhaps the exception of the H atom positional parameter for Na_2PtH_6 (Fig. 2b). In particular, the lattice parameter decreases linearly with decreasing size of the ionic radius of *A*. The H atom *x* parameter increases linearly and approaches ¼ (calculated value: 0.246) for *A*=Li. This leads to a peculiar situation when analyzing interatomic distances (Fig. 2c). The Pt–H distance in the octahedral complex ion is around 1.65 Å and virtually not affected by *A*. As a consequence distances between H atoms within the octahedral units (H–H(1)) and in between (H–H(2)) – which are considerably different for *A*=Na–Cs – become almost identical for Li_2PtH_6 (2.35 and 2.43 Å, respectively). This is shown in Fig. 3 where the structures of the two end members, Li_2PtH_6 and Cs_2PtH_6, are compared. As a matter of fact, the substructure of H atoms in Li_2PtH_6 approaches closely that of O atoms in the cubic perovskite structure and Li attains an almost regular cuboctahedral coordination by H atoms.

The "strained" situation of the Li_2PtH_6 structure is also apparent when comparing computed formation energies (referring to 0 K) for the reaction $2AH+Pt+2H_2=A_2PtH_6$ (Fig. 2d). For *A*=Cs, Rb, K the value is very similar, around −3 eV. It decreases to −2.5 eV for Na_2PtH_6 and becomes just −1.7 eV for Li_2PtH_6. The temperature-dependent Gibbs free energy ($\Delta G_{(T)}H_2$) for a H_2 gas molecule with respect to 0 K is around −0.32 eV at 300 K [29]. Therefore Li_2PtH_6 should represent a thermodynamically stable compound at room temperature and ambient pressure [30].

Li_2PtH_6 decomposes at temperatures between 150 and 200 °C when heating in a 1 bar Ar atmosphere for 20 h. The X-ray powder pattern of the decomposition product obtained at 200 °C shows very broad reflections which can be related to fcc-Pt. These reflections constitute – somewhat sharpened – also the pattern of the 250 °C decomposition product. When decomposing Li_2PtH_6 at 300 °C trigonal Li_yPtH_x [31], LiH and a small amount of $LiPt_7$ can be indentified in the powder pattern of the product. Thus, the thermal behavior of Li_2PtH_6 is different from $Li_5Pt_2H_9$, which decomposes quantitatively to Li_2PtH_2 (with zero-valent Pt) and LiH at 220 °C when applying the same conditions [32]. Li_2PtH_2 decomposes at 280 °C to Li_yPtH_x [32]. Finally, somewhat surprising is the observation that Li_2PtH_6 degrades only slowly outside a protective atmosphere while the heavier homologues are extremely air/moisture sensitive.

In Fig. 4 we compare the IR spectra of Na_2PtH_6, Li_2PtH_6 and Li_2PtD_6. The vibrational properties of K_2PtH_6 and Rb_2PtH_6 have been extensively studied previously both by optical (IR and

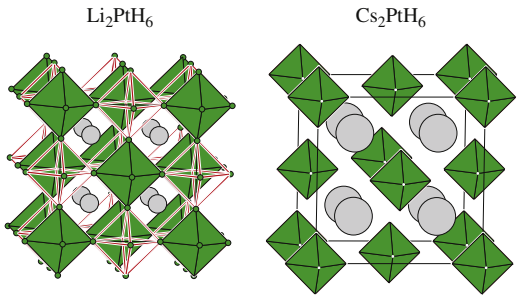

Fig. 3. Structure of Li_2PtH_6 (left) and Cs_2PtH_6 (right). The H atom framework in Li_2PtH_6 is emphasized by red lines. (For interpretation of the references to color in this figure legend, the reader is referred to the web version of this article.)

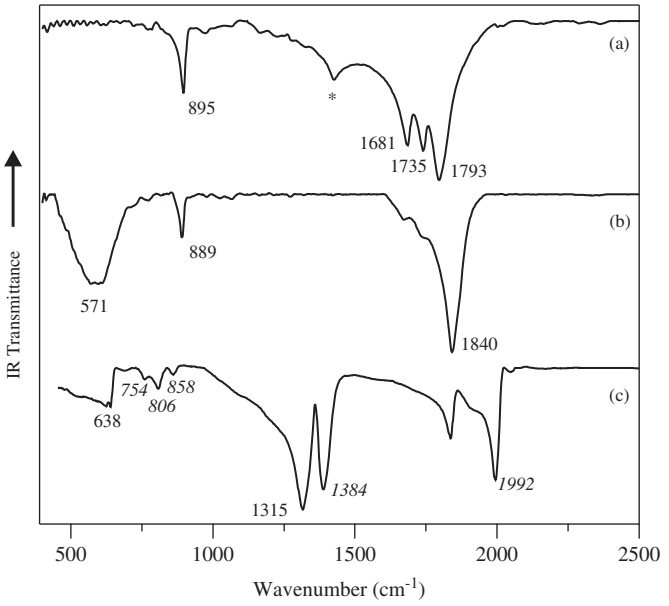

Fig. 4. IR spectra of Na_2PtH_6 (a), Li_2PtH_6 (b), and "Li_2PtD_6" (c). "Li_2PtD_6" has an estimated composition $Li_2PtH_{1.5}D_{4.5}$ The asterisk in spectrum (a) denotes an impurity associated with the decomposition of extremely air/moisture sensitive Na_2PtH_6. Italicized wave numbers in spectrum (c) refer to modes for heteroleptic $[PtH_nD_{6-n}]^{2-}$. The unlabeled mode at 1840 cm^{-1} in spectrum (c) belongs to $[PtH_6]^{2-}$ (cf. spectrum (b)).

Raman) and by inelastic neutron scattering (INS) spectroscopy [14,33,34]. The findings from these studies are excellent points of reference.

The IR spectrum of Na_2PtH_6 (Fig. 4a) shows the expected T_{1u} (asymmetric) Pt–H stretching and bending modes at 1793 and 895 cm^{-1}, respectively. The stretching mode appears peculiarly split which – in exactly the same way – is also observed for the K and Rb compounds [34]. This feature has been lately attributed to extra bands observable because of Fermi resonance [33]. The Pt–H stretching/bending mode frequencies increase slightly when going from the Rb (1743/877 cm^{-1}) to the K compound (1748/881 cm^{-1}). This trend continues with the Na compound, however, the amount of increase is substantially larger.

The Pt–H stretching mode for Li_2PtH_6 appears at 1840 cm^{-1}, which represents a further substantial increase compared to Na_2PtH_6, while the frequency of the bending mode (889 cm^{-1}) is lower than that for the Na compound (Fig. 4b). The feature of additional bands accompanying the stretch, which is characteristic for the heavier homologues, is only vaguely recognizable for Li_2PtH_6. The most obvious difference compared to the heavier homologues is the occurrence of a broad and intense band at low frequencies (with a maximum around 571 cm^{-1}). The origin of this band is not clear. It is unlikely that it relates to libration or translation. Librations (or torsions) of PtH_6^{2-} octahedra are inactive in optical spectroscopy for the heavier homologues [14]. In the INS spectrum of Rb_2PtH_6 the librational mode is at 366 cm^{-1} and translational modes are observed at around 100 cm^{-1} [14]. Although translation has an IR active T_{1u} component and the mass difference between Li and Rb is huge, its frequency should not rise above 400 cm^{-1} ($\sqrt{m_{Rb}}/\sqrt{m_{Li}} \approx 3.5$). Therefore we attribute this band to an impurity, perhaps stemming from oxidation/hydrolysis of the side product $LiPt_7$ ($LiPt_7H_x$).

The spectrum of Li_2PtD_6 (Fig. 4c) reveals the presence of heteroleptic D/H complexes. Apparently, the deuterium source BD_3ND_3 used for its synthesis had not been completely proton-exchanged. Earlier Bublitz et al. [34] prepared purposely a series of mixed complexes $K_2[PtH_nD_{6-n}]$ for spectroscopic studies. Based on their results the bands at 1992 and 1384 cm^{-1} can be assigned to Pt–H and Pt–D stretches, respectively, in heteroleptic $Li_2[PtH_nD_{6-n}]$. The bends of such complexes appear in the region 700–900 cm^{-1}. The Pt–D stretch for homoloeptic Li_2PtD_6 is at 1315 cm^{-1} (corresponding to an isotopic shift of 1.399), while the bend should coincide with the sharp edge of the broad intensity feature at low frequencies. This edge is at 638 cm^{-1} (corresponding to an isotopic shift of 1.393); the bending mode is camouflaged by – what we think – a broad impurity band. The intensity ratio of stretches stemming from heteroleptic $[PtH_nD_{6-n}]^{2-}$ and homoleptic PtD_6^{2-} complexes in the IR spectrum of Fig. 4c matches very well that for $K_2[PtH_nD_{6-n}]$ $n=1.5$ reported by Bublitz et al. [34]. Thus we assume that our isotopomer has a similar composition.

3. Conclusions

Li_2PtH_6, the missing member of the complex transition metal hydride series A_2PtH_6 (A=alkali metal), has been prepared by high pressure hydrogenations employing multi-anvil (MA) techniques. According to powder X-ray diffraction analysis Li_2PtH_6 is isostructural to its heavier homologues and crystallizes in the cubic K_2PtCl_6 structure. However, whereas PtH_6^{2-} octahedral complexes are well separated for the heavier homologues, H–H distances within and between octahedra become almost equal for Li_2PtH_6. Therefore the Li_2PtH_6 structure may likewise be regarded as a defective perovskite structure where half of the octahedrally coordinated atoms (cations) are missing. The IR observable T_{1u} Pt–H stretching mode is highest for A=Li (1840 cm^{-1}).

High pressure hydrogenations offer exciting prospects for metal hydrides synthesis because of the sharply increased activity of hydrogen above 1 GPa. We facilitated this kind of synthesis for MA techniques by introducing ammonia borane as superior hydrogen source and by employing large-volume pressure cells. The advantage of BH_3NH_3 is a well-defined decomposition to inert residuals under high pressure and the easy access of BD_3ND_3 for the preparation of deuterized samples. Employing large-volume pressure cells ensures appreciable quantities of reaction product despite the fact that a considerable fraction of sample volume is occupied by the hydrogen source.

4. Methods

High pressure hydrogenations were carried out in a 6–8 Walker-type multi-anvil (MA) high pressure module [35]. Reactants were LiH (Aldrich, powder, 95%), LiD (from reacting Li (Aldrich, rod, 99.99%) with D_2 at a pressure of 5 bar at 750 °C for 12 h), NaH (Aldrich, powder, 95%), Pt (Alfa Aesar, powder, 99.9%), BH_3NH_3, and BD_3ND_3. BH_3NH_3 was synthesized according to the procedure described in Ref. [36]. BD_3ND_3 was obtained by reacting $NaBD_4$ with ammonium formate and subsequent deuteration of the amine protons with D_2O (according to Ref. [37]. Here an additional deuteration cycle should have been performed to achieve complete proton exchange.

The preparation of the sample capsule was preformed in an Ar-filled glove box (O_2 concentration < 0.1 ppm). Mixtures of metal hydride(deuteride) and Pt with a total amount of about 100 mg were pressed into a pellet, which was placed in a NaCl capsule between two pellets of BH_3NH_3(BD_3ND_3). Subsequently the NaCl capsule was sealed. The sealed capsule was taken out from the glove box and positioned inside a graphite furnace. This arrangement was then placed together with a zirconia thermal

insulating sleeve in a magnesia octahedron with 18 mm edge length. Samples were pressurized with 25 mm tungsten carbide cubes truncated to 12 mm edge length. After reaching the target pressure the samples were heated slowly to temperatures between 450 and 500 °C and quenched after 60 min by turning off the power to the furnace (quench rate ~200 °C/min and at approximately constant pressure). When BH_3NH_3 decomposes, the sample volume shrinks considerably which may cause a blowout. We found that a slow heating rate (1 °C/min) reduces substantially the risk for such a blowout. The temperature was measured close to the sample using a thermocouple type C (W5%Re–W26%Re wire) in an Al_2O_3 sleeve. Afterward, the pressure was released over a period of several hours and the sample recovered in the glove box. Typically the three-pellet arrangement of the sample preparation is still recognizable after the run. All hydrides/deuterides had a grey color (from contamination of small amounts of Pt or $LiPt_7$) and could be easily separated from the surrounding white residual of decomposed BH_3NH_3(BD_3ND_3). Preparations for subsequent sample analysis were performed in the glove box.

The products Li_2PtH_6, Li_2PtD_6 and Na_2PtH_6 were analyzed by powder X-ray diffraction and IR spectroscopy. Samples were ground, loaded into 0.3 mm capillaries, and measured on a Bruker D8 Advance diffractometer fitted with an incident beam Ge monochromator (transmission geometry; Cu$K\alpha_1$ radiation). Lattice parameters were obtained from least-squares refinement of the measured and indexed lines of the corresponding powder diffractograms [38]. The reflection positions were corrected by use of an internal Si standard. The Rietveld refinements were performed with the TOPAS software [39]. For the Rietveld analysis, the following parameters were refined: background, unit cell, sample displacement, profile, isotropic atomic displacement parameters, and absorption correction [40]. Fourier-transform infrared spectroscopy (FTIR) investigations were carried out on a Bruker IFS 66v/s instrument. KBr pellets were prepared in the glove box and transferred in a closed container to the spectrometer.

For thermal decomposition experiments 10–20 mg amounts of Li_2PtH_6 sample were pressed into a pellet, which was loaded in a sealable stainless steel container in the glove box. The steel container was heated for 20 h at different temperatures between 150 and 300 °C.

Theoretical calculations were performed in the framework of the frozen core all-electron projected augmented wave (PAW) method [41], as implemented in the program VASP [42]. The energy cut-off was set to 500 eV. Exchange and correlation effects were treated by the generalized gradient approximation (GGA), usually referred to as PW91 [43]. The integration over the Brillouin zone was done over a $15 \times 15 \times 15$ Monkhorst-Pack grid [44]. Total energies were converged to at least 1 meV/atom. For all A_2PtH_6 systems the H atom positional parameter was optimized for a fixed volume of the unit cell. By repeating this process for different volumes the equilibrium cell and positional parameter are determined from the global minimum energy.

Acknowledgments

This research has been supported by the ACS Petroleum Research Fund under the Grant no. 45796-AC10 and the National Science Foundation through Grants DMR-0638826 and CHE-0742006. We are grateful to Dr. Stewart F. Parker (ISIS facility, STFC Rutherford Appleton Laboratory (UK)) for valuable advice in the analysis of IR spectra.

References

[1] K. Yvon, Chimia 52 (1998) 613.
[2] W. Bronger, J. Alloys Compd. 229 (1995) 1.
[3] T.K. Firman, C.R. Landis, J. Am. Chem. Soc. 120 (1998) 12650.
[4] M. Olofsson-Mårtensson, U. Häussermann, J. Tomkinson, D. Noreus, J. Am. Chem. Soc. 122 (2000) 6960.
[5] U. Häussermann, H. Blomqvist, D. Noreus, Inorg. Chem. 41 (2002) 3684.
[6] W. Bronger, G. Auffermann, Chem. Mater. 10 (1998) 2723.
[7] D. Noreus, K.W. Törnroos, A. Börje, T. Szabo, W. Bronger, H. Spittank, G. Auffermann, P. Müller, J. Less-Common Met. 139 (1988) 233.
[8] W. Bronger, G. Auffermann, J. Alloys Compd. 228 (1995) 119.
[9] W. Bronger, P. Müller, D. Schmitz, H. Spittank, Z. Anorg. Allg. Chem. 516 (1984) 35.
[10] W. Bronger, G. Auffermann, J. Alloys Compd. 219 (1995) 45.
[11] W. Bronger, G. Auffermann, Angew. Chem. Int. Ed. 33 (1994) 1112.
[12] W. Bronger, G. Auffermann, Z. Anorg. Allg. Chem. 621 (1995) 1318.
[13] W. Bronger, L.A. Brassard, Angew. Chem. Int. Ed. 34 (1995) 898.
[14] S.F. Parker, S.M. Bennington, A.J. Ramirez-Cuesta, G. Auffermann, W. Bronger, H. Herman, K.P.J. Williams, T. Smith, J. Am. Chem. Soc. 125 (2003) 11656.
[15 (a) H. Hemmes, A. Driessen, R.J. Griessen, C Phys., Solid State Phys. 19 (1986) 3571;
(b) A. Driessen, P. Sänger, H. Hemmes, R. Griessen, J. Phys., Condens. Matter 2 (1990) 9797.
[16] (a) H.-K. Mao, P.M. Bell, Science 203 (1979) 1004;
(b) J.V. Badding, R.J. Hemley, H.-K. Mao, Science 253 (1991) 421;
(c) R. Burtovyy, M. Tkacz, Solid State Commun. 131 (2004) 169.
[17] (a) N. Kawai, S. Endo, Rev. Sci. Instrum. 41 (1970) 1178;
(b) H. Huppertz, Z. Kristallogr. 219 (2004) 330.
[18] L.G. Khvostantsev, V.N. Slesarev, V.V. Brazhkin, High Pressure Res. 24 (2004) 371;
(b) L.G. Khvostantsev, V.N. Slesarev, Phys. Usp. 51 (2008) 1059.
[19] M. Tkacz, Defect Diffusion Forum 208-209 (2002) 107.
[20] E. Stoyanov, U. Häussermann, K. Leinenweber, High Pressure Res. 30 (2010) 175.
[21] (a) V.E. Antonov, J. Alloys Compd. 330-332 (2002) 110;
(b) V.E. Antonov, M. Baier, B. Dorner, V.K. Fedotov, G. Grosse, A.I. Kolesnikov, E.G. Ponyatovsky, G. Schneider, F.E. Wagner, J. Phys.: Condens. Matter 14 (2002) 6427.
[22] Y. Fukai, J. Alloys Compd. 404-406 (2005) 7.
[23] Y. Fukai, N. Okuma, Phys. Rev. Lett. 73 (1994) 1640.
[24] H. Saitoh, A. Machida, Y. Katayama, K. Aoki, Appl. Phys. Lett. 93 (2008) 151918.
[25] (a) E. Rönnebro, N. Kitamura, T. Sakai, J. Alloys Compd. 358 (2003) 216;
(b) J. Chen, T. Sakai, N. Kitamura, H.T. Takeshita, N. Kuriyama, J. Am. Chem. Soc. 123 (2001) 6193;
(c) A. Kamegawa, Y. Goto, R. Kataoka, H. Takamura, M. Okada, Renew. Energy 33 (2008) 221;
(d) H. Takamura, H. Kakuta, Y. Goto, A. Kamegawa, M. Okada, Mater. Trans. 42 (2001) 1301;
(e) D. Kyoi, T. Sato, E. Rönnebro, N. Kitamura, A. Ueda, M. Ito, S. Katsuyama, S. Hara, D. Noréus, T. Sakai, J. Alloys Compd. 372 (2004) 213.
[26] J. Nylén, T. Sato, E. Soignard, J.L. Yarger, E. Stoyanov, U. Häussermann, J. Chem. Phys. 131 (2009) 104506.
[27] M.G. Hu, J.M. van Paasschen, R.A. Geanangel, J. Inorg., Nucl. Chem. 39 (1977) 2147.
[28] W. Bronger, G. Klessen, P. Müller, J. Less-Common Met. 109 (1985) L1.
[29] X. Ke, I. Tanaka, Phys. Rev. B 71 (2005) 024117.
[30] This estimate neglects zero point energies, the effect of pressure and the temperature dependence of the internal energy.
[31] B. Nacken, W. Bronger, J. Less-Common Met. 52 (1977) 323.
[32] W. Bronger, L.A. Brassard, Z. Anorg. Allg. Chem 622 (1996) 462.
[33] S.F. Parker, Coord. Chem. Rev. 254 (2010) 215.
[34] D. Bublitz, G. Peters, W. Preetz, G. Auffermann, W. Bronger, Z. Anorg. Allg. Chem. 623 (1997) 184.
[35] D. Walker, M.A. Carpenter, C.M. Hitch, Am. Mineral. 75 (1990) 1020.
[36] Y. Lin, W.L. Mao, V. Drozd, J.H. Chen, L.L. Daemen, J. Chem. Phys. 129 (2008) 234509.
[37] V.M. Parvanov, G.K. Schenter, N.J. Hess, L.L. Daemen, M. Hartl, A.C. Stowe, D.M. Camaioni, T. Autrey, Dalton Trans. (2008) 4514.
[38] P.-E. Werner, Ark. Kemi 31 (1969) 513.
[39] Bruker AXS, TOPAS V4: General profile and structure analysis software for powder diffraction data, User's Manual, Karlsruhe, Germany, 2008.
[40] T.M. Sabine, B.A. Hunter, W.R. Sabine, C.J. Ball, J. Appl. Crystallogr. 31 (1998) 47.
[41] (a) P.E. Blöchl, Phys. Rev. B 50 (1994) 17953;
(b) G. Kresse, J. Joubert, Phys. Rev. B 59 (1999) 1758.
[42] (a) G. Kresse, J. Hafner, Phys. Rev. B 47 (1993) 558;
(b) G. Kresse, J. Furthmüller, Phys. Rev. B 54 (1996) 11169.
[43] J.P. Perdew, J. Wang, Phys. Rev. B 45 (1992) 13244.
[44] H.J. Monkhorst, J.D. Pack, Phys. Rev. B 13 (1976) 5188.